1   Robust Genome-Wide Ancestry Inference for Heterogeneous Datasets and
2   Ancestry Facial Imaging based on the 1000 Genomes Project

3

4   Jairui Li[1,2,*], Tomas Gonzalez[3], Julie D. White[3], Karlijne Indencleef[1,4], Hanne Hoskens[1,5], Alejandra
5   Ortega Castrillon[1,2], Nele Nauwelaers[1,2], Arslan Zaidi[3], Ryan J. Eller[6], Torsten Günther[7], Emma M.
6   Svensson[7], Mattias Jakobsson[7], Susan Walsh[6], Kristel Van Steen[5,8,9], Mark D. Shriver[3], Peter
7   Claes[1,2,5,10,11*]

8   [1]Medical Imaging Research Center, MIRC, University Hospitals Leuven, Leuven, Belgium

9   [2]Department of Electrical Engineering, ESAT/PSI, KU Leuven, Leuven, Belgium

10 [3]Department of Anthropology, The Pennsylvania State University, University Park, Pennsylvania, US

11 [4]Department of Neurosciences, Experimental Otorhinolaryngology, KU Leuven, Leuven, Belgium

12 [5]Department of Human Genetics, KU Leuven, Leuven, Belgium

13 [6]Department of Biology, Indiana University-Purdue University Indianapolis, Indianapolis, US

14 [7]Department of Organismal Biology, Uppsala University, Norbyvägen 18C, 75236, Uppsala, Sweden

15 [8]Medical Genomics Research Unit, GIGA-R, University of Liège, Belgium

16 [9]Walloon Excellence in Life sciences and Biotechnology (WELBIO), Belgium;

17 [10]Murdoch Childrens Research Institute, Melbourne, Victoria, Australia

18 [11]Department of Biomedical Engineering, University of Oxford, United Kingdom

19 * corresponding authors: Jiarui.li@kuleuven.be, peter.claes@kuleuven.be

20 Medical Imaging Research Center, University Hospitals Leuven, Herestraat 49 – box, 7003, 3000
21 Leuven, Belgium. Phone: +32 16 34 90 24,

22 **Short Title:** Robust Genome-Wide Ancestry Inference for Heterogeneous Datasets

Abstract

Accurate inference of genomic ancestry is critically important in human genetics, epidemiology, and related fields. Geneticists today have access to multiple heterogeneous population-based datasets from studies collected under different protocols. Therefore, joint analyses of these datasets require robust and consistent inference of ancestry, where a common strategy is to yield an ancestry space generated by a reference dataset. However, such a strategy is sensitive to batch artefacts introduced by different protocols. In this work, we propose a novel robust genome-wide ancestry inference method; referred to as SUGIBS, based on an unnormalized genomic (UG) relationship matrix whose spectral (S) decomposition is generalized by an Identity-by-State (IBS) similarity degree matrix. SUGIBS robustly constructs an ancestry space from a single reference dataset, and provides a robust projection of new samples, from different studies. In experiments and simulations, we show that, SUGIBS is robust against individual outliers and batch artifacts introduced by different genotyping protocols. The performance of SUGIBS is equivalent to the widely used principal component analysis (PCA) on normalized genotype data in revealing the underlying structure of an admixed population and in adjusting for false positive findings in a case-control admixed GWAS. We applied SUGIBS on the 1000 Genome project, as a reference, in combination with a large heterogeneous dataset containing auxiliary 3D facial images, to predict population stratified average or ancestry faces. In addition, we projected eight ancient DNA profiles into the 1000 Genome ancestry space and reconstructed their ancestry face. Based on the visually strong and recognizable human facial phenotype, comprehensive facial illustrations of the populations embedded in the 1000 Genome project are provided. Furthermore, ancestry facial imaging has important applications in personalized and precision medicine along with forensic and archeological DNA phenotyping.

Author Summary

Estimates of individual-level genomic ancestry are routinely used in human genetics, epidemiology, and related fields. The analysis of population structure and genomic ancestry can yield significant insights in terms of modern and ancient population dynamics, allowing us to address questions regarding the timing of the admixture events, and the numbers and identities of the parental source populations. Unrecognized or cryptic population structure is also an important confounder to correct for in genome-wide association studies (GWAS). However, to date, it remains challenging to work with heterogeneous datasets from multiple studies collected by different laboratories with diverse genotyping and imputation protocols. This work presents a new approach and an accompanying open-source software toolbox that facilitates a robust integrative analysis for population structure and genomic ancestry estimates for heterogeneous datasets. Given that visually evident and easily recognizable patterns of human facial characteristics covary with genomic ancestry, we can generate predicted ancestry faces on both the population and individual levels as we illustrate for the 26 1000 Genome populations and for eight eminent ancient-DNA profiles, respectively.

Introduction

Scientists today have access to large heterogeneous datasets from many studies collected by different laboratories with diverse genotyping and imputation protocols. The joint analysis of these datasets requires a robust and consistent inference of ancestry across all datasets involved, where one common strategy is to yield an ancestry space generated by a reference set of individuals (1). Based on open-research initiatives such as the 1000 Genome project (1KGP) (2), HapMap project (3), Human Genome Diversity project (HGDP) (4), and the POPRES dataset (5), the potential exists to create reference ancestry latent-spaces at different levels of interest, from worldwide inter-continental to fine-scale intra-continental ancestry. A reference ancestry space allows the researcher to collate multiple datasets facilitating analyses that are more advanced. For example, reference ancestry spaces can be used to infer the population structure of samples with family structure or cryptic relatedness (1) and to investigate the genetic similarity between ancient DNA and modern human genomes (6). They also have the potential to correct for population structure in a genome-wide association study (GWAS) on heterogeneous and admixed samples. Of final interest is the association of auxiliary data (e.g. specific phenotypes, such as 3D facial shape used in this work) present in internally collected datasets with ancestral variations captured by a reference space. This requires the projection of the collected datasets into a reference space, followed by an association of the projection scores with the auxiliary data presented.

Methodologically, the idea is to construct an ancestry latent-space from a reference dataset and to enable the projection of new cases from other datasets that follow the mainstream of the reference dataset. Starting from genome-wide single nucleotide polymorphisms (SNPs), PCA and analogous dimension reduction techniques on normalized genotype data are popular strategies used in this context (7,8). However, in construction of an ancestry space, these approaches are known to be sensitive to outliers (7,9). In addition and more importantly, in projecting new cases onto an ancestry space, PCA produces patterns of misalignment (for example, "shrinkage" patterns where projected cases tend to falsely gravitate towards the center of the ancestry space) due to missing data, missing heterozygotes, and genotyping along with imputation errors, which is misleading without careful interpretation (1). Therefore, stringent quality control and data filters are typically in place to remove individual outliers and SNP data with high missing rates or not in Hardy-Weinberg equilibrium (HWE). However, in heterogeneous datasets, in contrast to homogeneous datasets, such data filters are harder to define, and potentially remove SNP data related to population structure. Furthermore, genotyping and imputation batch artefacts, not detected by quality control and different from one protocol to another, typically remain and still affect an integrative analysis of ancestry.

In this work, we propose a novel robust genome-wide ancestry inference (referred to as SUGIBS) based on the spectral (S) decomposition of an unnormalized genomic (UG) relationship matrix generalized by an Identity-by-State (IBS) similarity degree of individuals' matrix. Robustness against outliers, during ancestry space construction, is obtained by absence of specific sample statistics (e.g. allele frequencies). Furthermore, SUGIBS provides a robust projection of new samples, from different studies, onto a reference SUGIBS space. During projection, the IBS similarity degree of individuals to project to individuals in the reference dataset acts as a correcting term for missing genotypes and errors, and most interestingly this correction is on an individual-by-individual basis. We test the robustness of SUGIBS and compare its performance to PCA and Multi-Dimensional Scaling (MDS) in revealing the underlying structure of an admixed population and adjusting for false positive findings

3

102   in a simulated case-control admixed GWAS. Using the 1KGP as reference dataset, and an additional
103   heterogeneous dataset containing 3D facial images, we apply SUGIBS to construct ancestry faces that
104   illustrate the ancestral variation captured in the 1KGP. Additionally, we reconstruct the ancestry faces
105   for eight high-coverage ancient DNA genomes further illustrating the potential of the work. Based on
106   the results, our method facilitates a robust integrative analysis for ancestry estimation in
107   heterogeneous datasets.

Results

109   In the first experiment, we investigated the robustness of SUGIBS in comparison to traditional
110   approaches, in particular PCA using normalized or unnormalized genotype data and MDS using IBS
111   distances as they are implemented in PLINK 1.9 (10), against individual outliers in a reference dataset.
112   For this purpose, we first selected all unrelated individuals from the CEU and TSI populations in the
113   HapMap 3 project (Belmont et al., 2003) and used SUGIBS, PCA, unnormalized PCA (UPCA) and MDS
114   to illustrate the first and second latent dimensions as ancestry components (Figure 1, top row). In
115   contrast to the traditionally used normalized genotypes in PCA, UPCA used unnormalized genotypes
116   that were not centralized around the mean and were not standardized to a variance equal to one. As
117   expected, PCA, MDS and SUGIBS are able to differentiate between both populations along the first
118   ancestry component. The first component of UPCA seems to aggregate the average pattern of SNPs
119   instead of the differentiation between two groups. Surprisingly, with PCA a single outlier (NA11917)
120   that was not expected during the selection of both populations already affected the second ancestry
121   component. Subsequently, we randomly selected one individual from four different and additional
122   populations (CHB, GIH, MEX and YRI) as "outliers" in the dataset. Figure 1, bottom row, illustrates the
123   first two ancestry components of the four methods constructed on the dataset with outliers, where
124   all four approaches clearly separate the outliers. Using PCA, in contrast to MDS, UPCA and SUGIBS the
125   clear distinction between CEU and TSI is lost within the first two ancestry components, as they mainly
126   capture variations due to the outliers. The main reason for robustness in UPCA, MDS and SUGIBS is
127   that these three methods use unnormalized genotype data and therefore do not rely on specific
128   sample statistics (e.g. allele frequencies), that otherwise increase the influence of outlier variation.
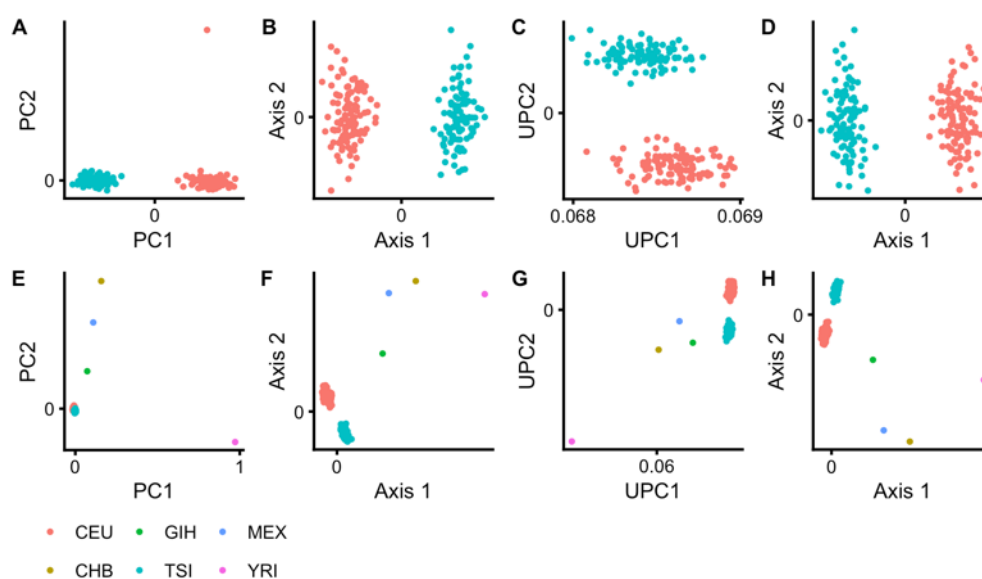
129

130   *Figure 1: Robustness against individual outliers during the construction of an ancestry space. Top row,*
131   *the first two ancestry components for A) PCA, B) MDS, C) UPCA and D) SUGIBS using the CEU and TSI*

132   *populations from the HapMap 3 project. Bottom row, the first two ancestry components for E) PCA, F)*
133   *MDS, G) UPCA and H) SUGIBS using the CEU and TSI populations from the HapMap 3 project, but with*
134   *randomly selected single individuals from four different and additional populations (CHB, GIH, MEX*
135   *and YRI) as "outliers".*

136   In a second experiment, we projected (Methods, equation 4) new samples on an ancestry space, based
137   on the 1KGP as reference dataset, to investigate the robustness of SUGIBS in comparison to PCA and
138   UPCA against typical artifacts of different laboratory protocols. Note that, since the first component
139   of UPCA just aggregated the average pattern as seen in experiment 1, we started UPCA from the
140   second component onwards. Also note that, MDS does not allow for a straightforward projection of
141   new samples on a reference space and was therefore excluded. As samples to project, we randomly
142   assigned all 1,043 individuals of 51 populations from the HGDP dataset (4) into two equally-sized
143   samples, one unchanged and one modified, respectively. To investigate the influence of different rates
144   of missing data, we randomly masked 5% of the SNP genotypes as missing in the modified population
145   (See Methods). For the influence of different rates of errors, we partially changed SNP genotypes with
146   minor allele frequency (MAF) less than 5% in the modified population (See Methods). Note that this
147   was done knowing that more imputation errors are observed in SNPs with a MAF of 5% and less (11).
148   We projected both HGDP populations onto the PCA, UPCA and SUGIBS reference spaces as defined by
149   the 1KGP. In PCA, the simulated artefacts generated "shrinkage" and "shifting" patterns of
150   misalignment in the first two projected ancestry components (Figure 2, top row), for missing and
151   erroneous genotypes, respectively. UPCA was only influenced by missing genotypes (Figure 2, middle
152   row). In contrast, SUGIBS was not influenced by missing or erroneous genotypes (Figure 2, bottom
153   row). Figure 3 summarizes the normalized root-mean-square deviations (NRMSD) of the first eight
154   axes of SUGIBS, UPCA and PCA of the modified HGDP population over 100 simulations. SUGIBS is
155   significantly more robust than PCA in the presence of missing and genotyping/imputation errors in
156   new data for which ancestry needs to be inferred, by projecting it into a reference space.
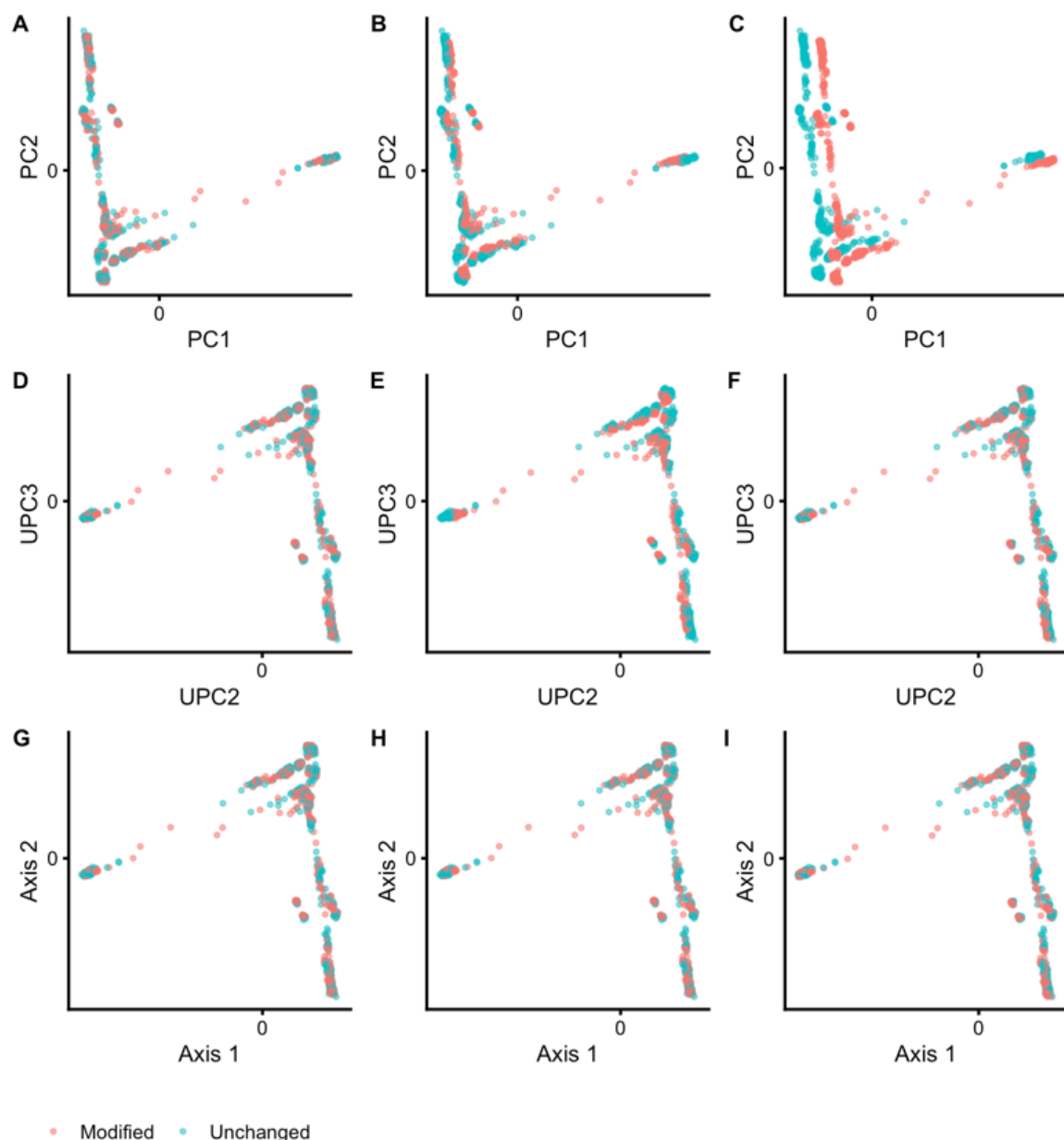
Figure 2: Robustness against batch artefacts during the projection of samples onto an ancestry space. Top row, the first two ancestry components of PCA using the original genotypes A), missing genotypes B) and modified genotypes C). Middle row, the second and third ancestry components of UPCA using the original genotypes D), missing genotypes E) and modified genotypes F). Bottom row, the first two ancestry components of SUGIBS using the original genotypes G), missing genotypes H) and modified genotypes I).
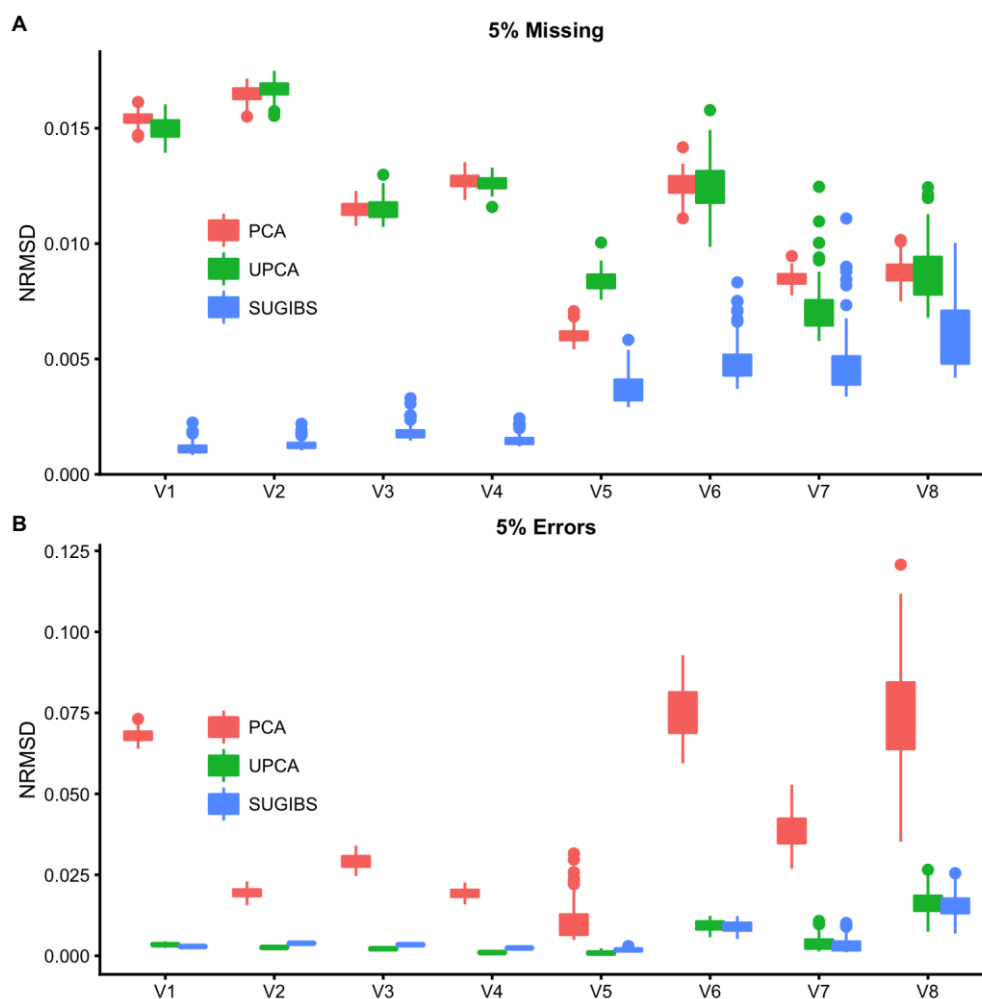
165

166

Figure 3: Normalized root-mean-square deviation (NRMSD) of the top eight axes of PCA, UPCA and SUGIBS. NRMSD measures the root-mean-square differences (RMSD), for the modified HGDP population only between the scores on ancestry axes generated using the original genotypes (error free) and the modified genotypes (with simulated errors, A) missing genotypes and B) erroneous genotypes). The RMSD values were normalized by the range of the ancestry axes generated using the original genotypes, so that NRMSD of the three methods (PCA, UPCA and SUGIBS) are comparable.

In a third experiment, following the work of Galinsky et al. (12), we investigated the ability of SUGIBS compared to PCA and MDS in representing admixture. We simulated data at 10,000 random independent SNPs for 1,000 individuals from a recent admixture of two populations, 50% from each population on average with divergences $F_{st} = \{0.001, 0.005, 0.01, 0.05, 0.1\}$, from an intra-European difference to an intercontinental difference (13). Because the admixture contains only one dimension of population structure, only the first component of variation is of interest. Figure 4 presents the absolute correlations between the first component of PCA, MDS and SUGIBS and the simulated ancestry proportions over 100 runs. When the F_{st} divergence between two populations is lower than 0.05, the correlation between the SUGIBS component and the ancestry proportion is similar to that of MDS, but a little lower than PCA. We noticed that when $F_{st} \leq 0.01$, all three methods have a reduced

183   performance to reveal the underlying admixture and when $F_{st} > 0.01$, all three methods perform
184   perfectly.
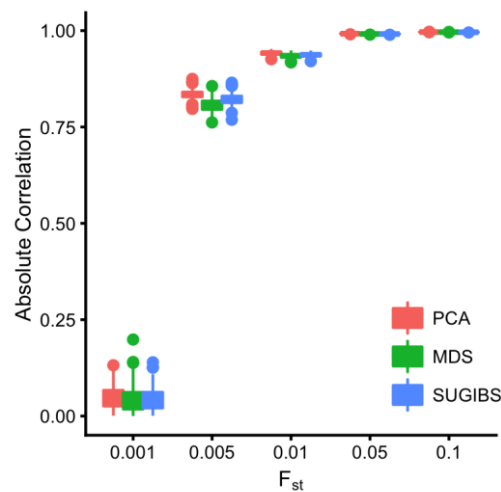
186   *Figure 4: Capturing simulated admixture in function of F_{st}. X-axis represents the different levels of Fst*
187   *investigated. The Y-axis represents the absolute correlation of the first component in PCA, MDS and*
188   *Spectral-IBS with the simulated ancestry proportion. The higher the correlation the better a method is*
189   *able to capture the underlying admixture.*

190   Following the work of Price et al. (14), we also simulated a case-control GWAS to investigate if the
191   population structure inferred by SUGIBS can be used for correcting population stratification as a
192   confounder. Only low divergences between the two populations $F_{st} = \{0.001, 0.005, 0.01\}$, were
193   tested, because for larger divergences all three methods would perform the same as deducted from
194   the previous experiment. Tests were conducted with a logistic regression under four different
195   correction scenarios: 1) no population for stratification correction (Naïve), 2) PCA, 3) MDS and 4)
196   SUGIBS, using a likelihood ratio test for the significance of each genetic marker. The experiment was
197   conducted 100 times, with average proportions of SNPs detected as significant shown in Table 1.
198   These results indicate that in a single dimensional population structure, correcting using MDS, SUGIBS
199   and PCA perform similarly, both in terms of Type I error and power. All three methods failed to correct
200   the population stratification when $F_{st} = 0.001$, which is consistent with the failure of the three
201   methods in revealing the admixture structure in the previous experiment. Finally, these results are in
202   line with the results in (14).

203

	Naive	PCA	MDS	SUGIBS
$F_{st} = 0.001$				
Random	0.0002	0.0001	0.0001	0.0001
Differentiated	0.9960	0.4483	0.6370	0.5200
Causal	0.5295	0.4779	0.4865	0.4807
$F_{st} = 0.005$				
Random	0.0009	0.0001	0.0001	0.0001
Differentiated	0.9980	0.0002	0.0003	0.0002
Causal	0.5226	0.4249	0.4255	0.4253
$F_{st} = 0.01$				
Random	0.0030	0.0001	0.0001	0.0001
Differentiated	0.9971	0.0001	0.0001	0.0001
Causal	0.5166	0.4227	0.4230	0.4229

Table 1: Proportion of associations reported as statistically significant ($P < 0.0001$) by logistic regression using a likelihood ratio test. Random SNPs with no association to the disease were generated by simulating random drift with F_{st} divergence. Differentiated SNPs with no association to the disease were generated by assuming population allele frequencies of 0.8 of ancestry 1 and 0.2 of ancestry 2. Causal SNPs were generated by combining a multiplicative disease risk model while simulating the random drift with the same F_{st} as the random SNPs. See methods for more details on the parameters.

Putting SUGIBS to practice, we projected 2,882 unrelated individuals from a large admixed and heterogeneous dataset containing individuals from varying ancestries (the PSU cohort, see Methods) and eight famous ancient DNA samples onto the first 25 SUGIBS axes established from the 26 populations in the 1KGP. Shown in Figure 5 and S1 (a), the first two ancestry components separate the African (AFR) and East Asian (ESA) populations from the remaining populations, as indicated by the population labels given in the 1KGP. The next two ancestry components in Figure 5 and S1 (b) separate the South Asian (SAS) population and visualizes the admixture in the Admixed American (AMR) population, respectively. In figure 5 and S1 (c), the sixth ancestry component captures different subpopulations in the EAS population. In Figure 5 and S1 (d), the seventh ancestry component is driven by African subpopulations and the separated European subpopulation on the eighth ancestry component is the population from Finland (FIN). The projected PSU cohort is indicated by gray dots in Figure 5 and S1 and overall it is observed that they overlay well with a wide range of ancestry variations in the 1KGP confirming the heterogeneous and admixed nature of the PSU dataset. However, some populations in the 1KGP are less covered by the PSU cohort, such as the population of Finland in Europe and some African subpopulations on ancestry components seven and eight (Figure 5 d).
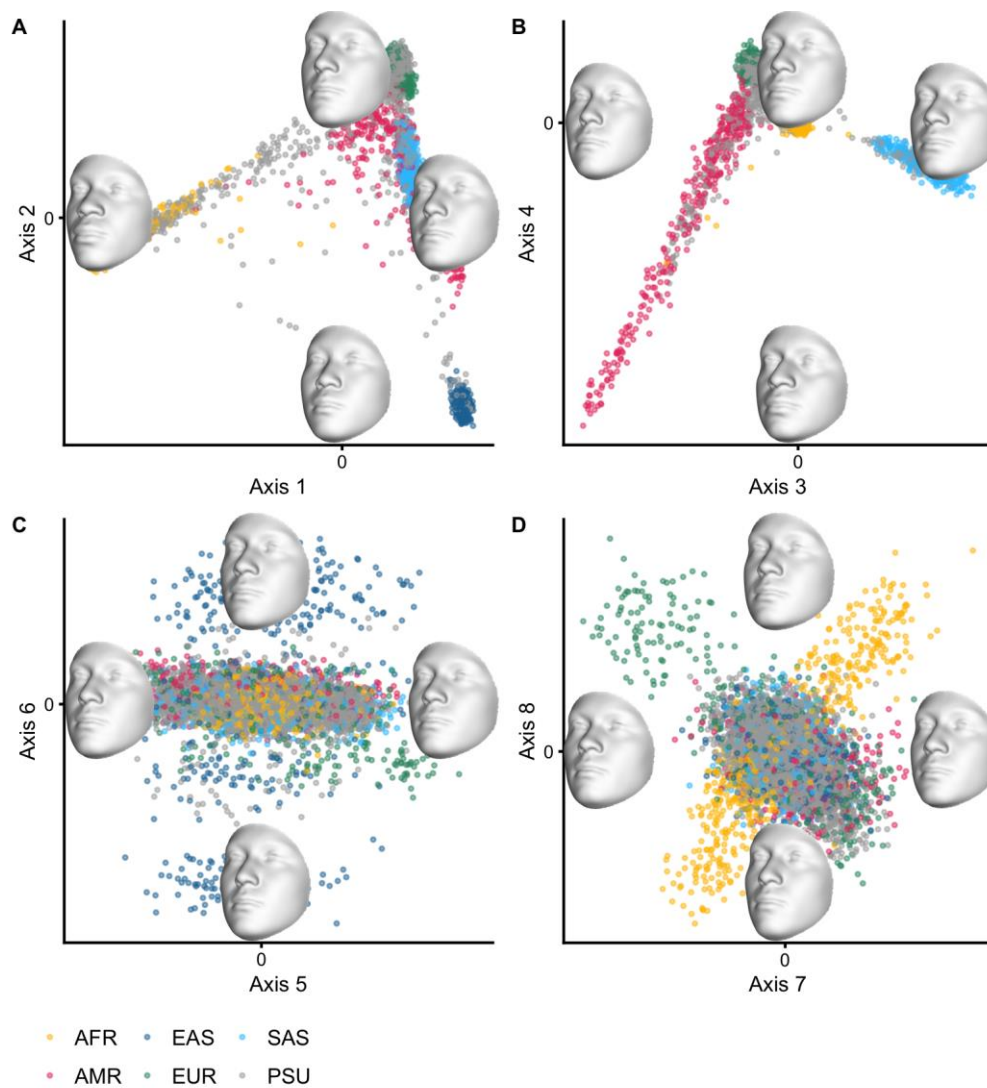
Figure 5: Top eight SUGIBS axes of 1KGP and projections of the PSU cohort. Grouped populations of the 1KGP are coloured dots. The projected PSU cohort are represented by grey dots. The faces illustrate opposing variations along each of the ancestry components and are not associated to any of the 1kG populations in particular (these are shown in Figure 6).

Based on the visually strong and recognizable human facial phenotype, we generated comprehensive illustrations of the population structure embedded in the 1KGP. Using the first 25 SUGIBS scores of the PSU cohort onto the ancestry components of the 1KGP, we fitted a partial least squares regression (PLSR) to model facial variations in function of each of the first eight ancestry components (Figure 5). Strong facial differences are observed for ancestry components 1-4, whilst perceptually smaller differences occur in components 5-8. This is most likely due to a lower overlap of the PSU cohort with these ancestry components. Subsequently, we reconstructed the ancestry population average face from each of the 26 populations in the 1KGP (Figure 6), and ancestry faces specific for eight high-coverage ancient DNA profiles (Figure 7). The facial images in Figures 5, 6 and 7, are perceptually easy to confirm the expected variations in facial shape in function of genetic ancestry including admixtures. For the ancient DNA profiles labeled in Figure 7, it is observed that their projections within the 1kG ancestry is consistent with the geographical locations where these samples were discovered and what is currently known about these samples (Supplementary Table S1).

244

245

Figure 6: Ancestry population average faces for each of the 26 populations in the 1KGP positioned according to geographical origin. The values for sex, BMI and age in the PLSR model were set to 0 (sexless), 20 and 25, respectively.
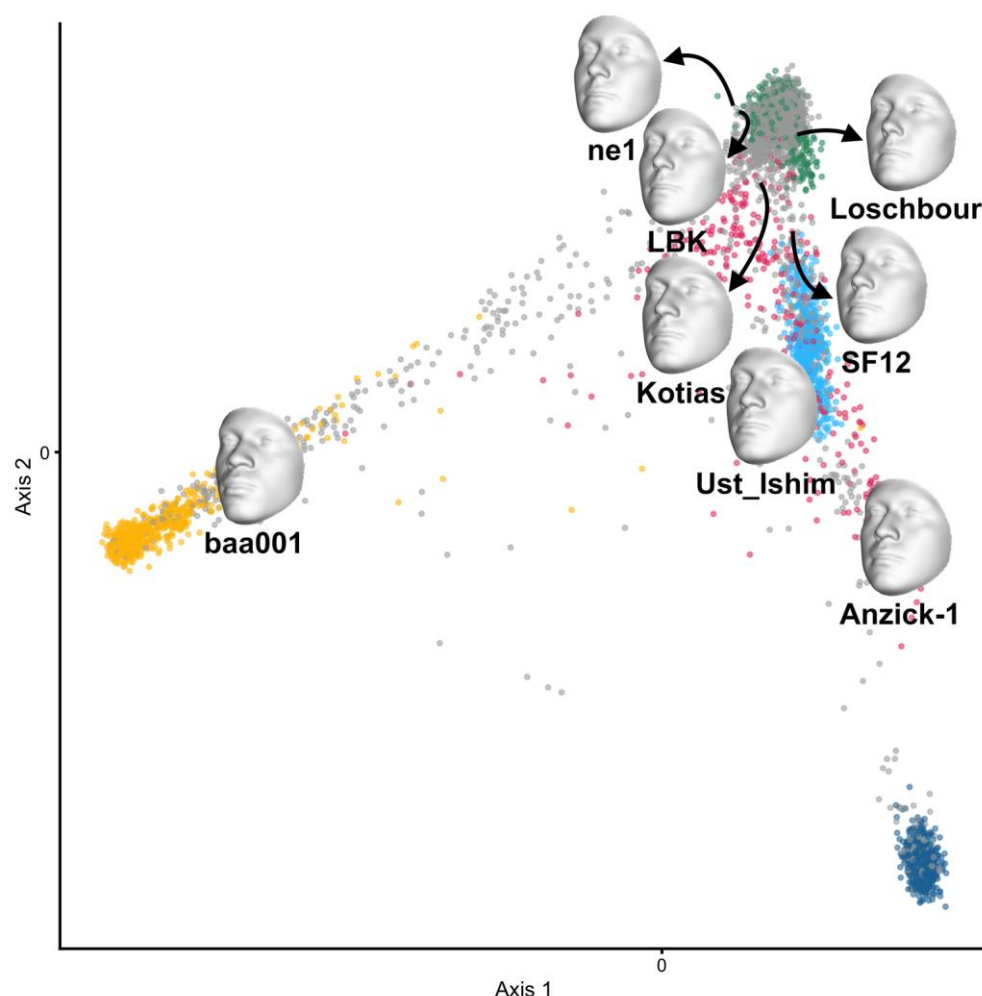
Figure 7: Ancestral facial reconstructions for eight ancient DNA profiles. For these reconstructions, the sex was known from the DNA profile and taken into account in the PLSR model. The values for BMI and age were 20 and 25, respectively.

Discussion

Accurate inference of population structure and individual global ancestry is of critical importance in human genetics, epidemiology, and related fields (15,16). The analysis of population structure in itself can yield significant insights in terms of population dynamics, both in modern and ancient populations (17–19). Through inspection of ancestry components as well as distances in genetic latent spaces created by, for example, Principal Component Analysis (PCA), it is possible to infer patterns of gene flow and population movements through time. Furthermore, the inclusion of various populations in genome-wide association studies (GWAS) could increase statistical power and make a better contributions to our understanding of the genetics of complex traits for the human population as a whole (20). However, the widely used approach of PCA and analogous techniques are sensitive to outliers, when constructing ancestry spaces, and produce patterns of misalignment due to artifacts of different laboratory protocols when new samples are projected onto a reference ancestry space (1,7,9). We propose a robust alternative for genome-wide ancestry inferencing, referred to as SUGIBS. Our results confirm the erroneous influences in PCA based ancestry estimations that are misleading without careful interpretation. In constructing an ancestry space SUGIBS, shares the same robustness against individual outliers as MDS or related spectral graph approaches (21). Furthermore, and more

12

269   importantly, during dataset projections SUGIBS is robust against typical artefacts from different
270   laboratory protocols. In addition, SUGIBS achieved the same performance, under error-free conditions,
271   as PCA in revealing the underlying structure of an admixed population and avoiding false positive
272   findings in a simulated case-control GWAS with an admixed population.

273   Like MDS and SUGIBS, PCA is also a "spectral" method, in which the edge similarity between
274   individuals is simply the covariance of normalized genotypes, commonly referred to as the genomic
275   relationship matrix (22). However, this covariance similarity used in PCA depends on the allele
276   frequencies as a non-robust sample statistic to normalize the genotypes, which causes sensitivity to
277   individual outliers. Note that in our experiments on PCA without using allele frequencies (UPCA)
278   robustness against individual outliers was observed. Among the "spectral" methods, some other
279   robust alternatives were introduced to infer population structure, including a modified genomic
280   relationship (21,23). MDS or related spectral graph approaches (21) using IBS and Allele Sharing
281   Distance (ASD) similarities between individuals (available in PLINK (10)) are also a robust alternative
282   against individual outliers, as illustrated in our results. IBS and ASD are unnormalized distances, and
283   thus less influenced by outliers. However, MDS and the modified genomic relationship used in (21,23),
284   both lack the ability to project new samples on an already established reference ancestry space.
285   Alternatively, it might be possible to use one of the many robust PCA approaches that have been
286   investigated for general data (24–26) as well as genetic data (27). However, in most study data
287   processing protocols, robust approaches are usually used for outlier detection rather than inferring
288   population structure, which is done by classical PCA after excluding outliers (27). This is for example,
289   a standardly used option in the popular EIGENSOFT software (7). Note that, when establishing an
290   ancestry space from a reference dataset, it remains good practice to identify and remove individual
291   outliers, if they are of no further interest.

292   The main contribution of SUGIBS is robustness against batch artifacts of different laboratory and data
293   processing protocols when projecting new samples onto a reference ancestry space. In the case of
294   missing genotypes, smaller absolute PC scores, and smaller UPC scores are wrongfully generated
295   during the projection of samples. These smaller and decreased scores lead to the "shrinking" and
296   "shifting" patterns as observed in the results. (Note that this is not to be confused with PCA shrinkage
297   due to high dimensional and large-scale data, which is dealt with using shrinkage eigenvalue
298   estimations as recently implemented in EIGENSOFT). However, to correct for this, the projected
299   SUGIBS score matrix is weighted by the reference degree matrix, which captures the similarity
300   between the data to be projected and the reference data (see Methods). This weighting of projected
301   SUGIBS scores equally corrects for the effects of genotyping and imputation errors, as demonstrated
302   in the results. To the best of our knowledge, we are currently not aware of another related approach
303   that offers the same robustness. Based on the results, we argue that SUGIBS is a solid alternative to
304   PCA and MDS and requires less stringent data filters to operate. Our implementation of SUGIBS uses
305   the randomized singular value decomposition algorithm (28), that is also used in FastPCA (12). This
306   makes the algorithm computationally tractable for datasets with tens of thousands of individuals and
307   millions of SNPs. SUGIBS is available as part of an open-source in-house Matlab^{TM} library, referred to
308   as SNPLIB, in which we used PLINK binary file formats as input, and provide FastPCA, logistic GWAS
309   and all other methods and simulations mentioned throughout this work. Furthermore, SUGIBS can
310   easily be incorporated into existing and interesting extensions to derive common ancestry estimations
311   in datasets with non-overlapping genetic variants (1), or genotyping-by-sequencing data (29), or

312 population structure inference in presence of relatedness (30), or in iterative schemes to obtain global
313 to fine-scale ancestry estimations (31).

314 There are a few points of discussion and future investigations. First, a genetic similarity measure
315 between pairs of individuals aims to identify how they are related and different measures exist for
316 ancestry estimations (e.g. IBS, ASD, Identity-by-descent, normalized covariance) (22). Commonly used
317 similarity measures are normalized, just like the traditional approach of PCA on normalized genotype
318 data, to take the genetic composition of individuals along with the rest of the sample into account. A
319 normalization does have the advantage that individuals within the same population are more similar
320 to each other than to individuals in other populations (22). In other words, the distinction between
321 populations increases, which improves population identification by clustering algorithms. However,
322 when the normalization is performed incorrectly clustering efforts might be inaccurate. Furthermore,
323 as seen in our results, such a normalization increases the influence of individual outliers. Finally, in
324 contrast to homogeneous datasets, normalization of genotype data in heterogeneous datasets is
325 challenging depending on whether the dataset is unlabeled or not, imbalanced or not, and with high
326 admixture or not. Starting from unlabeled data, unsupervised clustering approaches such as
327 ADMIXTURE (32) and STRUCTURE (33), iteratively identify the populations individuals belong to and
328 update the normalization accordingly. However, this involves additional parameters to set and tune,
329 the most important one being the amount of clusters expected in the data. Without prior knowledge
330 on how to set these parameters, this can turn into a challenging task. With highly admixture data, any
331 clustering of global ancestry into populations is even questionable. In these situations, only local
332 ancestry estimations, using chromosome painting approaches (34) for example, are meaningful.
333 Alternatively, in the future, we want to investigate the use of a reference ancestry space as
334 constructed in this work, without assigning individuals to specific populations, in estimating
335 normalized genotype data on an individual-by-individual basis. I.e., an ancestry space from
336 unnormalized genotype data is a good first step unbiased by any sample statistics, to further deduct
337 statistics related to individual genotype profiles. For example, (35) propose the Robust Unified Test
338 for Hardy-Weinberg Equilibrium in the context of an admixed population, which also makes use of
339 individual-level adjustments for ancestry. Second, future investigations of the methodology also
340 include the influence of LD pruning and data filtering for SNP selection. Population admixture is one
341 of the main sources for LD between SNPs, therefore we prefer to avoid excessive LD pruning before
342 applying SUGIBS. As stated in (22) any data pruning or filtering is bound to loose information related
343 to population structure. For example, less common variants are typically lost in data filtering, but
344 these might contain valuable information about population structure (22). Since SUGIBS is robust and
345 computationally tractable, any data filtering can be minimized. Third, another future investigation
346 involves the determination of the number of relevant or significant components in SUGIBS, for which
347 we provide a preliminary suggestion that compares the spectrum of the data observed with that of a
348 simulated homogenous dataset assuming linkage equilibrium (LE) and Hardy-Weinberg Equilibrium
349 (Supplementary Text S1).

350 In application of SUGIBS we used the human face, which is a powerful phenotype to visualize and
351 illustrate underlying genetic ancestry variations. Indeed, faces are easy to recognize, interpret, and
352 validate the outcomes based on everyone's expert knowledge in facial perception. The faces
353 illustrating the ancestry components of the 1KGP in this work overlay well with the provided
354 population labels. Therefore, they can also provide a means to interpret ancestry variations in a
355 heterogeneous dataset in absence of population labels. It is important to note that an ancestry face,

356 as referred to in this work, for each of the 26 1kG populations and ancient DNA profiles are faces that
357 reflect a population's or an individual's genetic background and sex. In other words, ancestry faces
358 are not individually specific faces, but average faces that simply visualize the ancestry background of
359 a DNA profile. Related work on facial prediction from DNA (36,37), also show that sex and ancestry
360 are the primary factors driving the estimation of facial shape from DNA.

361 Ancestry facial predictions have good value in a range of applications. In archeology, ancestry faces
362 reconstructed from ancient DNA profiles, as done in this work, is of strong interest. Generally, for
363 ancient DNA profiles, missing data is abundantly present, making SUGIBS an interesting technique to
364 be used. Note that, the ancestry faces are limited to modern facial constructs, due to the
365 contemporary facial data used. However, they can help to bring ancient DNA profiles into the context
366 of present-day populations for which facial images (e.g. open-source facial databases, Google images,
367 etc.) are available but DNA is not. Furthermore, there is a good relationship between the face and the
368 skull (38,39), such that ancestry faces can be used to compare against skeletal remains. In the future,
369 it is of interest to deploy our work on datasets of 3D skeletal craniofacial surfaces extracted from
370 Computer Tomography (CT) or Magnetic Resonance Imaging (MRI). In medicine, and more particularly
371 in oral and maxillofacial surgery, the surgical reconstruction of a patient's face benefits from a proper
372 notion of normal facial shape (40). In the next five to 20 years, whole genome sequencing will become
373 the standard of care in clinics and a patient-specific ancestry face provides a personalized norm of
374 facial shape towards precision medicine in surgical planning. Finally, in forensics, an ancestry facial
375 prediction circumvents the often legally debated reporting of ancestry proportions of a probe DNA
376 profile in a criminal investigation. In France, for example, DNA phenotyping of externally visible traits
377 is legally allowed, since such traits are considered to be public. However, and in contrast, genomic
378 ancestry proportions, as typically reported in forensic DNA testing, is considered to be private
379 information and cannot be used during criminal investigations. We agree that ancestry proportions
380 are not an externally visible characteristic of an individual. The construction of ancestry proportions
381 is also inherently flawed by labelling the individual into so-called parental populations. Furthermore,
382 such numeric information is hard to interpret and use by a forensic investigator. The reconstruction
383 of an ancestry face on the other hand, avoids needing to explicitly label a DNA profile in function of
384 parental populations and provides a visual feedback to an investigator that is perceptually useful, even
385 in admixed cases. A future challenge in forensics does involve the ability to reconstruct ancestry faces
386 using often limited and contaminated DNA material.

387 In conclusion, SUGIBS is a novel approach to construct an ancestry space from a reference dataset and
388 to project new samples from heterogeneous datasets for a consistent and robust inference of
389 individual ancestry. The main contributions involve robustness against outliers during the construction
390 of an ancestry space, and robustness against batch artefacts during the projection of new samples
391 into an ancestry space. Therefore, SUGIBS is a solid alternative to PCA and MDS and facilitates a robust
392 integrative analysis for population structure and ancestry estimations for heterogeneous datasets.
393 Based on the visually strong and recognizable human facial phenotype, comprehensive illustrations of
394 genomic ancestry variations were provided for different populations in the 1KGP and for eight
395 eminent ancient-DNA profiles. Ancestry facial imaging from genome data has interesting future
396 applications in personalized and precision medicine along with forensic and archeological DNA
397 phenotyping.

398

Materials and Methods

SUGIBS latent-space construction: Given a dataset with N individuals and M SNPs, we first create an unnormalized genotype (UG) matrix $\boldsymbol{X}_{M \times N}$ with additive genotype coding (aa = -1, Aa = 0, AA = 1 and missing = 0). The UG relationship matrix is then defined as $\boldsymbol{G} = \frac{1}{M}\boldsymbol{X}^T\boldsymbol{X}$. Note that an unnormalized additive genotype coding has only three values (-1, 0, 1) and does not produce extreme values, which occurs with normalized additive genotype encoding schemes (typically used in PCA) due to small minor allele frequencies and in the context of individual outliers.

From $\boldsymbol{W}_{N \times N}$, the IBS similarity matrix of the same dataset used to create $\boldsymbol{G}$, the similarity degree of an individual can be defined as $d_{ii} = \sum_{j=1}^{N} w_{ij}$. We followed the algorithm implemented in PLINK to calculate the IBS similarity so that:

IBS	AA	Aa	aa
AA	2	1	0
Aa	1	2	1
aa	0	1	2
N/A	0	0	0

However, in contrast to the calculations in PLINK, we do not normalize the IBS similarity matrix with missingness scores. This results in a similarity degree matrix $\boldsymbol{D}$ defined as the diagonal matrix with $d_{11}, \ldots, d_{NN}$ on the diagonal. We use $\boldsymbol{D}$ to define generalized eigenvectors $\boldsymbol{v}_k = (v_{k1}, \ldots, v_{kn})^T$ of $\boldsymbol{G}$ with corresponding generalized eigenvalues λ_k , and $\lambda_1 \geq \lambda_2 \geq \lambda_3 \geq \ldots$:

$$\boldsymbol{G}\boldsymbol{v}_k = \lambda_k \boldsymbol{D}\boldsymbol{v}_k \tag{1}$$

Similar to UPCA, the first generalized eigenvector of $\boldsymbol{D}$ and $\boldsymbol{G}$ simply represents the average pattern of all SNPs. Therefore, we start from the second generalized eigenvector and define the kth component of SUGIBS to be the $k+1$th generalized eigenvector of $\boldsymbol{G}$ and $\boldsymbol{D}$, $\boldsymbol{v}_{k+1}$.

By multiplying $\boldsymbol{D}^{-\frac{1}{2}}$ on both sides of equation (1), we obtain:

$$\boldsymbol{D}^{-\frac{1}{2}}\boldsymbol{G}\boldsymbol{D}^{-\frac{1}{2}}\boldsymbol{D}^{\frac{1}{2}}\boldsymbol{v}_k = \lambda_{k+1}\boldsymbol{D}^{-\frac{1}{2}}\boldsymbol{v}_k \tag{2}$$

Subsequently, we observe that the eigenvector $\boldsymbol{v}'_k = \boldsymbol{D}^{\frac{1}{2}}\boldsymbol{v}_k$ of $\boldsymbol{D}^{-\frac{1}{2}}\boldsymbol{G}\boldsymbol{D}^{-\frac{1}{2}} = \frac{1}{M}\boldsymbol{D}^{-\frac{1}{2}}\boldsymbol{X}^T\boldsymbol{X}\boldsymbol{D}^{-\frac{1}{2}}$ can be obtained from the singular value decomposition (SVD) of the matrix $\hat{\boldsymbol{X}} = \boldsymbol{X}\boldsymbol{D}^{-\frac{1}{2}} = \boldsymbol{U}\boldsymbol{\Sigma}\boldsymbol{V}'^T$, where $\boldsymbol{v}'_k$ is also the ith right singular vector with singular value $\sigma_k = \sqrt{M\lambda_{k+1}}$, $\boldsymbol{\Sigma}$ is a $N \times N$ diagonal matrix, $\boldsymbol{U}$ is a $M \times N$ matrix with all the left singular vectors and $\boldsymbol{V}'$ is a $N \times N$ matrix with all the right singular vectors.

Denoting $\boldsymbol{U}_k = \{\boldsymbol{u}_2, \ldots, \boldsymbol{u}_{k+1}\}$ and $\boldsymbol{\Sigma}_k = diag\{\sigma_2, \ldots, \sigma_{k+1}\}$, the corresponding left singular vectors and the singular values of the first k SUGIBS components $\boldsymbol{V}_k = \boldsymbol{D}^{-\frac{1}{2}}\boldsymbol{V}'_k = \boldsymbol{D}^{-\frac{1}{2}}\{\boldsymbol{v}_2, \ldots, \boldsymbol{v}_{k+1}\}$, we have the following equation:

16

428
$$V_k = D^{-\frac{1}{2}}V'_k = D^{-1}S_k = D^{-1}X^T L_k = D^{-1}X^T U_k \Sigma_k^{-1} \tag{3}$$

429   Thus, we denote $L_k = U_k \Sigma_k^{-1}$ as the SUGIBS loading matrix for the first k SUGIBS components and

430     $S_k = X^T U_k \Sigma_k^{-1}$ as the unnormalized SUGIBS score matrix.

431   We proposed a preliminary method to select proper number of components which compared the
432   spectrum of the observed data with that of the simulated data, assuming HWE and Linkage Equilibrium
433   (see Supplement note).

434   ***SUGIBS dataset projection:*** Given the SUGIBS loadings L_k from a reference dataset with N individuals
435   and M SNPs and given a new dataset with $\widetilde{N}$ individuals and the same set of SNPs as the reference
436   sample, we denote the unnormalized genotype matrix of the new dataset as $\widetilde{X}$. We then define the
437   reference degree $\tilde{d}_{ii} = \sum_j^N \widetilde{w}_{ij}$, where $\widetilde{w}_{ij}$ is denoted as the IBS similarity between the ith individual
438   in the target dataset and the jth individual in the reference dataset. The reference similarity degree
439   matrix $\widetilde{D}$ of the new dataset is a diagonal matrix with $\tilde{d}_{11}, \dots, \tilde{d}_{\widetilde{N}\widetilde{N}}$ on the diagonal. For the first k
440   SUGIBS components, the projected score matrix of the target dataset is then obtained as:

441
$$\widetilde{V}_k = \widetilde{D}^{-1}\widetilde{S}_k = \widetilde{D}^{-1}\widetilde{X}^T L_k = \widetilde{D}^{-1}\widetilde{X}^T U_k \Sigma_k^{-1} \tag{4}$$

442   In equation (4), the reference similarity degree matrix $\widetilde{D}$ acts as a normalization term correcting the
443   missing genotypes and errors in the samples to be projected. As an example, consider a rare SNP with
444   major allele *A* and minor allele *G*, and an individual with true genotype *AA* that is wrongfully coded as
445   *GG* for that particular SNP. Since the major genotype in the reference data of this SNP is *AA*, the
446   number of shared alleles of this SNP between this individual to the majority of individuals in the
447   reference dataset would reduce from 2 to 0. The unnormalized genotype coding of this person also
448   changes from 1 to -1. Thus, the influence of such a genotyping error on the unnormalized SUGIBS
449   score matrix $\widetilde{S}_k$ and the reference similarity degree matrix $\widetilde{D}$ are along the same direction so that the
450   final SUGIBS scores are corrected by $\widetilde{D}^{-1}$. Other typical batch artefact errors and missing genotypes
451   in the new dataset are corrected for in a similar way and, most interestingly, this correction is provided
452   on an individual by individual basis.

453   ***Genome-wide common SNP selection across datasets:*** We recommend the following procedure to
454   extract a common set of SNPs between a reference dataset and another dataset being projected, for
455   constructing SUGIBS ancestry spaces. First, we exclude all the indel, monomorphic, and multi-allelic
456   SNPs in both the reference dataset and the dataset to project. Subsequently, we extract the list of
457   SNPs common in both datasets. Based on this list, we further recommend a minor allele frequency
458   (MAF) filtering with a MAF threshold of 0.01 on the reference dataset using PLINK (10) as a quality
459   control step. We do not recommend Hardy-Weinberg disequilibrium (HWD) filtering since it is
460   probably the result of population admixture and thus useful for our purposes (41). Although
461   population admixture is one of the main sources for LD between SNPs, we still recommend LD pruning
462   since it is not unusual to have non-uniformly genotyped genomes. Similar to PCA, SUGIBS do not
463   explicitly model LD between SNPs so that misleading results might be generated without LD pruning.

464   ***Individual outlier robustness:*** The basic dataset that was used to investigate robustness against
465   individual outliers in a reference dataset, consists of the individuals from the CEU population (111
466   individuals) and the TSI population (102 individuals) from the HapMap 3 dataset (3), after excluding
467   non-founders. We randomly selected one individual as outlier from four other populations (CHB, MEX,

468   GIH, and YRI). These individuals specifically are NA18798 (CHB), NA19740 (MEX), NA21124 (GIH), and
469   NA19262 (YRI). After removing the monomorphic SNPs in each of these three datasets, we built
470   SUGIBS, MDS, UPCA and PCA spaces using 892,338 autosomal SNPs remaining in all three datasets.
471   We intentionally did not perform either minor allele frequency (MAF) filtering or HWE filtering on the
472   SNPs since many rare SNPs and SNPs violating HWE are due to the outliers and were therefore not
473   checked for during the testing for robustness.

474   ***Simulated laboratory artefacts:*** We used the 1000 Genomes Project dataset (2,504 unrelated
475   individuals from 26 populations) as the reference dataset to infer a PCA, UPCA and SUGIBS based
476   ancestry space. We used the HGDP dataset that analyzed genomic data from 1,043 individuals from
477   around the world as the dataset to project. First, we remapped the HGDP dataset from the NCBI36
478   (hg18) assembly to the GRCh37 (hg19) assembly using the NCBI Genome Remapping Service. Based
479   on the SNP selection procedure for SUGIBS as explained previously, we further performed a LD pruning
480   with a window size of 50, a moving step of 5 and a threshold $r^2 > 0.2$ for several times until no more
481   SNPS were excluded, following (12). LD pruning is a common practice when using PCA. Therefore, we
482   followed this additional step to make the results based on PCA, UPCA and SUGIBS comparable. We
483   finally selected 154,199 autosomal SNPs to construct the PCA, UPCA and SUGIBS ancestry spaces. We
484   then extracted the first eight PCA, UPCA and SUGIBS ancestry components from the reference dataset.
485   After extracting the same set of SNPs in the HGDP dataset, we took care to ensure that the alternate
486   alleles were the same as in the reference dataset.

487   Since PLINK binary file format stores the genotypes of four consecutive individuals in a single byte, we
488   assigned one of every two "bytes" (four individuals) into Population A and the other individuals into
489   Population B of the HGDP dataset. This resulted in 523 individuals for Population A and 520 individuals
490   for Population B. In order to simulate laboratory artefacts, we randomly masked 5% genotype calls as
491   missing and changed 5% genotype calls (e.g., from AA to Aa or aa) of the rare SNPs (MAF < 0.05) in
492   Population A. Random genotype masking and changing were also performed on the "byte" level, i.e.
493   four individuals at a time. For both genotyping masking and changing, we generated 100 datasets to
494   project on the 1kG reference ancestry space. Subsequently, we calculated the root-mean-square
495   deviations (RMSD) between the scores of the top eight PCA, UPCA and SUGIBS axes generated using
496   the original genotypes and the modified genotypes in Population A and further normalized them by
497   the range of the axes generated using the original genotypes so that normalized root-mean-square
498   deviations (NRMSD) across methods are comparable.

499   ***Simulated admixed population:*** Our admixture simulations were adapted from the section
500   "Simulation Framework" in (12). For a given SNP i, the ancestral allele frequency p_i was sampled from
501   a $Uniform(0.1,0.9)$ distribution. Population allele frequencies were generated by simulating random
502   drift in two populations of fixed effective size N_e for τ generations as p_{i1} and p_{i2}, whose initial values
503   were set to p_i. In each generation, the number of alternate alleles z_{i1} and z_{i2} were sampled from two
504   binomial distributions with $2N_e$ number of trials and p_{i1} and p_{i2} success probabilities. The population
505   allele frequencies were then updated by $p_{i1} = \frac{z_{i1}}{2N_e}$ and $p_{i2} = \frac{z_{i2}}{2N_e}$. For all simulations, population allele
506   frequency simulations were run for 20 generations and the effective population size N_e was calculated
507   for a target F_{st} by $F_{st} = -\log(1 - \frac{\tau}{2N_e})$ (42). This was done for $F_{st} = \{0.001, 0.005, 0.01, 0.05, 0.1\}$,
508   $N_e \approx \{10k, 2k, 1k, 200, 100\}$ with $\tau = 20$.

509   The ancestry proportions α_j were sampled from a $beta(0.5, 0.5)$ distribution so that the proportion

510   from each ancestry is 50% on average. For a given individual j with ancestry proportion of α_j from

511   Population one and $(1 - \alpha_j)$ from Population two, the individual allele frequency for SNP i was $p_i^j =$

512   $\alpha_j p_{i1} + (1 - \alpha_j) p_{i2}$ and the genotype was sampled from a binomial distribution with 2 trials and p_i^j

513   success probability. The Matlab^{TM} implementations for these simulations are also provided in our

514   SNPLIB library.

515   ***Simulated GWAS***: Our GWAS simulation is similar to the one carried out in (14). To simulate a case-

516   control GWAS, we generated 1,000 individuals from a population admixed from two ancestries. The

517   case-control status was simulated using a disease risk proportional to r^α, based on an ancestral risk

518   of $r = 3$. We generated three categories of SNPs (random, differentiating and causal) to compare the

519   performance of PCA, MDS, and SUGIBS in correcting for population stratification. For the first category

520   (random SNPs with no association to the disease), we generated the SNPs by simulating random drift

521   with a certain F_{st} divergence. For the second category (differentiated SNPs with no association), we

522   assumed population allele frequencies of 0.8 for ancestry one and 0.2 for ancestry two. For the third

523   category (causal SNPs), we generated SNPs by combining a multiplicative disease risk model while

524   simulating the random drift with the same F_{st} as the random SNPs.

525   We simulated the case-control status according to (7). For individuals with an ancestry proportion of

526   α from population one and $(1 - \alpha)$ from population two, the case-control status was simulated with

527   the probability of disease equal to $\frac{\log(r) r^a}{2(r-1)}$, which ensures an average value of 0.5 across all the values

528   of α (7).

529   For the case individuals, the population allele frequencies p_{i1} and p_{i2} of the causal SNP i were further

530   updated to $p_{i1}^* = \frac{R p_{i1}}{1 - p_{i1} + R p_{i1}}$ and $p_{i2}^* = \frac{R p_{i2}}{1 - p_{i2} + R p_{i2}}$ with a relative risk of $R = 3$, respectively. The

531   Matlab^{TM} implementations for these simulations are also provided in our SNPLIB library.

532   ***PSU cohort and 3D facial images:*** Study participants in the PSU cohort were recruited in the United

533   States through several studies based at The Pennsylvania State University under Institutional Review

534   Board (IRB) approved protocols (IRB #44929, #45727, #2503, #4320, #32341). 3D facial images were

535   taken using the 3dMD Face (3dMD, Atlanta, GA) and the Vectra H1 (Canfield, Parsippany, NJ) imaging

536   systems. Height and weight were measured using an Accustat stadiometer (Genentech, San Francisco,

537   CA), a clinical scale (Tanita, Arlington Heights, IL), or by self-report. Genotyping was conducted by

538   23andMe (23andMe, Mountain View, CA) on the v4 genome-wide SNP array and on the Illumina Multi-

539   Ethnic Global Array (MEGA). After filtering out SNPs with more than 10% missing genotypes, the

540   intersection of these two arrays compromised of approximately 600K SNPs. We removed individuals

541   with misclassified sex information, missing covariate data, and those with more than 10% missing

542   genotypes. Relatives were identified as pairs of individuals with an identity-by-state (IBS) value of at

543   least 0.8, after which one of each pair was randomly removed, resulting in a set of 2,882 individuals.

544   Genotypes were imputed to the 1000 Genomes Project Phase 3 reference panel, using SHAPEIT2

545   (Delaneau, Marchini, & Zagury, 2012) for prephasing of haplotypes and imputed using the Sanger

546   Imputation Server PBWT pipeline (Durbin, 2014; McCarthy et al., 2016).

547   3D facial images were imported into Matlab^{TM} 2016b in .obj wavefront format to perform spatially

548   dense registration (MeshMonk). After importing the images, five positioning landmarks were

549   indicated in the corners of the eye, the tip of the nose and the corners of the mouth to roughly align

550 the images into the same position. Subsequently, the images were cleaned by removing hair, ears,
551 and any dissociated polygons. A symmetrical anthropometric mask (43) of 7,160 landmarks was then
552 mapped onto the pre-processed images (44). This resulted in homologous spatially dense
553 configurations of quasi-landmarks per facial image. Reflected images were created by changing the
554 sign of the x-coordinate of the original mapped images. Both the original and the reflected remapped
555 faces were then superimposed following a generalized Procrustes superimposition to eliminate
556 differences in orientation, position and scale (45). Symmetrized images were created by averaging the
557 original and the reflected images.

558 Image quality control was performed to identify poorly remapped faces using two approaches. First,
559 as described in (46), outlier faces were identified by calculating Z-scores from the Mahalanobis
560 distance between the mean face and each individual face. Faces with Z-scores higher than 2 were
561 manually checked. Second, a score was calculated that reflects the missing data present in the image
562 due to holes, spikes, and other mesh artefacts that can be caused by facial hair or errors during the
563 pre-processing steps, for example. Images with scores indicating a high amount of missing data,
564 indicating large gaps in the mesh, were also manually checked. During the manual check, the images
565 were either classified as images of poor quality or were pre-processed again if possible and mapped
566 again.

567 ***Prediction of ancestry faces:*** Using 69,194 autosomal SNPs overlapping with the PSU cohort and the
568 ancient-DNA profiles, we constructed 25 SUGIBS ancestry components, which is theoretically
569 sufficient to separate 26 populations, from the 1000 Genomes project. Subsequently, we projected
570 the individuals from the PSU cohort and the ancient-DNA profiles onto the 1kG ancestry components.
571 Then, we fitted a partial least-squares regression (PLSR) model using the superimposed 3D facial
572 images with 7,160 quasi-landmarks collected in the PSU cohort as the response variables and the 25
573 projected SUGIBS scores of the PSU cohort together with three covariates (age, sex, and BMI) as the
574 explanatory variables.

575 Given specific ancestry scores on the ancestry components of the 1kG ancestry space, together with
576 age, BMI and sex (-1 (male), 0 (neutral sex) or 1 (female)), the PLSR model was used to predict ancestry
577 faces. To illustrate the ancestry components in Figure 7, we simply varied a single score along each
578 ancestry component separately, while keeping the scores on the other ancestry components fixed and
579 equal to the overall average scores in the PSU cohort together with values for age = 25, BMI = 20, and
580 sex = 0. For each of the 26 populations in the 1KGP, we calculated the average scores on each SUGIBS
581 ancestry component per population. These average scores together with values for age = 25, BMI =
582 20, and sex = 0, were used in the PLSR model to reconstruct the average ancestry faces for each of the
583 26 populations in the 1KGP. Diploid genotypes for the ancient genomes were called using GATK as
584 described in (47). The projected scores of the ancient-DNA profiles were used together with the
585 genome-derived sex values of each of the ancient individuals to reconstruct their ancestry faces in
586 Figure 7.

Acknowledgments

20

592 (WELBIO - Convention de Recherche n° WELBIO-CR-2015S-03R). The collaborators at the Penn State
593 University were supported in part by grants from the Center for Human Evolution and Development
594 at Penn State, the Science Foundation of Ireland Walton Fellowship (04.W4/B643), the United States
595 National Institute Justice (www.nij.gov; 2008-DN-BX-K125), and by the United States Department of
596 Defense (www.defense.gov). Torsten Günther is supported by the Swedish Research Council (2017-
597 05267).

598 *Ethics Statement:* Institutional review board (IRB) approval was obtained at each recruitment site and
599 all participants gave their written informed consent prior to participation; for children, written
600 consent was obtained from a parent or legal guardian. For the PSU cohort, the following local ethics
601 approvals were obtained: State College, PA (IRB #44929 and #4320 New York, NY (IRB #45727);
602 Urbana-Champaign, IL (IRB #13103); Dublin, Ireland; Rome, Italy; Warsaw, Poland; and Porto, Portugal
603 (IRB #32341); and Twinsburg, OH (IRB #2503)

604 *Author contributions:* J.L under supervision of P.C and K.V.S developed the SUGIBS methodology. J.L.
605 together with P.C. designed the experiments with input from K.V.S and M.D.S. J.L. under supervision
606 of P.C. and M.D.S conceptualized and implemented the ancestral facial imaging based on the 1000
607 Genome Project. J.W., T.G., A.Z., R.J.E. and S.W. curated the genomic data, including that of the PSU
608 cohort. M.D.S, J.W., K.I., H.H., N.N., and A.O.C collected and processed the 3D facial image data of the
609 PSU cohort. T.G., E.M.S., and M.J., provided and curated the eight ancient DNA profiles and were
610 involved in the ancestry facial imaging thereof. J.L and P.C wrote the manuscript with extensive input
611 from all co-authors.

612 *Competing interests:* The authors have no financial conflict of interest to report.

613 *Data and materials availability:* Most data used in this work originates from public open-source
614 projects, including the HapMap 3 project, 1000 Genome project and the HGDP dataset. For access to
615 this data, we refer to their respective webpages as indicated under the URL section.

616 The participants comprising the Penn State University dataset (PSU cohort) were not collected with
617 broad data sharing consent. Given the highly identifiable nature of both facial and genomic
618 information and unresolved issues regarding risk to participants, we opted for a more conservative
619 approach to participant recruitment. Broad data sharing of these collections would thus be in legal
620 and ethical violation of the informed consent obtained from the participants. This restriction is not
621 because of any personal or commercial interests. Additional details and a more confined sharing can
622 be requested from M.D.S.

623 An implementation of SUGIBS is freely available (see URL Section). This comprises a Matlab™ toolbox,
624 referred to as SNPLIB, and contains implementations of all the methods and simulations used in this
625 work. We also provide the resulting PLSR model, with demo script, to create Ancestry Facial images
626 for other open or in-house data collections (currently under construction). The spatially-dense facial
627 mapping software, referred to as MeshMonk, is available free of use for academic purposes (see URL
628 Section).

629 *URL's:*

630 HapMap 3 Data: https://www.genome.gov/10001688/international-hapmap-project/
631 1000 Genome Project: http://www.internationalgenome.org/

632   HGDP dataset: http://www.cephb.fr/hgdp/
633   SNPLIB: https://github.com/jiarui-li/SNPLIB
634   MeshMonk: https://github.com/TheWebMonks/meshmonk
635   NCBI Genome Remapping Service: https://www.ncbi.nlm.nih.gov/genome/tools/remap
636
637   **References**
638

639   1.   Wang C, Zhan X, Liang L, Abecasis GR, Lin X. Improved Ancestry Estimation for both Genotyping
640   and Sequencing Data using Projection Procrustes Analysis and Genotype Imputation. Am J Hum
641   Genet. 2015;

642   2.   Auton A, Abecasis GR, Altshuler DM, Durbin RM, Bentley DR, Chakravarti A, et al. A global
643   reference for human genetic variation. Nature. 2015;526(7571):68–74.

644   3.   Belmont JW, Hardenbol P, Willis TD, Yu F, Yang H, Ch'Ang LY, et al. The international HapMap
645   project. Nature. 2003 Dec;426(6968):789–96.

646   4.   Li JZ, Absher DM, Tang H, Southwick AM, Casto AM, Ramachandran S, et al. Worldwide human
647   relationships inferred from genome-wide patterns of variation. Science. 2008;319(5866):1100–
648   4.

649   5.   Nelson MR, Bryc K, King KS, Indap A, Boyko AR, Novembre J, et al. The Population Reference
650   Sample, POPRES: A Resource for Population, Disease, and Pharmacological Genetics Research.
651   Am J Hum Genet. 2008;

652   6.   Skoglund P, Malmström H, Omrak A, Raghavan M, Valdiosera C, Günther T, et al. Genomic
653   diversity and admixture differs for stone-age Scandinavian foragers and farmers. Science.
654   2014;

655   7.   Price AL, Patterson NJ, Plenge RM, Weinblatt ME, Shadick NA, Reich D. Principal components
656   analysis corrects for stratification in genome-wide association studies. Nat Genet.
657   2006;38(8):904–9.

658   8.   Patterson N, Price AL, Reich D. Population structure and eigenanalysis. PLoS Genet.
659   2006;2(12):2074–93.

660   9.   Clayton DG, Walker NM, Smyth DJ, Pask R, Cooper JD, Maier LM, et al. Population structure,
661   differential bias and genomic control in a large-scale, case-control association study. Nat
662   Genet. 2005 Nov;37(11):1243–6.

663   10.   Purcell S, Neale B, Todd-Brown K, Thomas L, Ferreira MAR, Bender D, et al. PLINK: A Tool Set
664   for Whole-Genome Association and Population-Based Linkage Analyses. Am J Hum Genet.
665   2007;81(3):559–75.

666   11.   Mitt M, Kals M, Pärn K, Gabriel SB, Lander ES, Palotie A, et al. Improved imputation accuracy of
667   rare and low-frequency variants using population-specific high-coverage WGS-based
668   imputation reference panel. Eur J Hum Genet. 2017 Jun 12;25(7):869–76.

669   12.   Galinsky KJ, Bhatia G, Loh PR, Georgiev S, Mukherjee S, Patterson NJ, et al. Fast Principal-
670   Component Analysis Reveals Convergent Evolution of ADH1B in Europe and East Asia. Am J
671   Hum Genet. 2016;98(3):456–72.

672 13. Nelis M, Esko T, Mägi R, Zimprich F, Toncheva D, Karachanak S, et al. Genetic structure of
673   europeans: A view from the north-east. PLoS ONE. 2009;

674 14. Price AL, Zaitlen NA, Reich D, Patterson N. New approaches to population stratification in
675   genome-wide association studies. Vol. 11, Nature Reviews Genetics. 2010. p. 459–63.

676 15. Bauchet M, McEvoy B, Pearson LN, Quillen EE, Sarkisian T, Hovhannesyan K, et al. Measuring
677   European Population Stratification with Microarray Genotype Data. Am J Hum Genet.
678   2007;80(5):948–56.

679 16. Cavalli-Sforza LL. Population Structure and Human Evolution. Proc R Soc B Biol Sci.
680   1966;164(995):362–79.

681 17. Cavalli-Sforza LL, Monozzi P, Piazza A. The History and Geography of Human Genes. Abridged e.
682   Princeton University Press. Princeton, NJ: Princeton University Press; 1994.

683 18. Rosenberg NA, Pritchard JK, Weber JL, Cann HM, Kidd KK, Zhivotovsky LA, et al. Genetic
684   structure of human populations. Science. 2002;298(5602):2381–5.

685 19. Nielsen R, Akey JM, Jakobsson M, Pritchard JK, Tishkoff S, Willerslev E. Tracing the peopling of
686   the world through genomics. Nature. 2017;541(7637):302–10.

687 20. Rosenberg NA, Huang L, Jewett EM, Szpiech ZA, Jankovic I, Boehnke M. Genome-wide
688   association studies in diverse populations. Nat Rev Genet. 2010;11(5):356–66.

689 21. Lee AB, Luca D, Roeder K. A spectral graph approach to discovering genetic ancestry. Ann Appl
690   Stat. 2012;6(1):179–202.

691 22. Lawson DJ, Falush D. Population Identification Using Genetic Data. Annu Rev Genomics Hum
692   Genet. 2012;13(1):337–61.

693 23. Zhang J, Niyogi P, Mcpeek MS. Laplacian eigenfunctions learn population structure. PLoS ONE.
694   2009;4(12).

695 24. Croux C, Filzmoser P, Oliveira MR. Algorithms for Projection-Pursuit robust principal
696   component analysis. Chemom Intell Lab Syst. 2007 Jun;87(2):218–25.

697 25. Croux C, Ruiz-Gazen A. High breakdown estimators for principal components: the projection-
698   pursuit approach revisited. J Multivar Anal. 2005 Jul;95(1):206–26.

699 26. Maronna R. Principal components and orthogonal regression based on robust scales.
700   Technometrics. 2005;

701 27. Liu L, Zhang D, Liu H, Arendt C. Robust methods for population stratification in genome wide
702   association studies. BMC Bioinformatics. 2013 Apr 19;14:132.

703 28. Halko N, Martinsson P-G, Tropp JA. Finding structure with randomness: Probabilistic algorithms
704   for constructing approximate matrix decompositions. SIAM Rev. 2009;53(2):217–88.

705 29. Dodds KG, McEwan JC, Brauning R, Anderson RM, Stijn TC, Kristjánsson T, et al. Construction of
706   relatedness matrices using genotyping-by-sequencing data. BMC Genomics. 2015;

707   30.   Conomos MP, Miller MB, Thornton TA. Robust inference of population structure for ancestry
708   prediction and correction of stratification in the presence of relatedness. Genet Epidemiol.
709   2015;

710   31.   Chaichoompu K, Yazew FA, Tongsima S, Shaw PJ, Sakuntabhai A, Van Steen K. IPCAPS: an R
711   package for iterative pruning to capture population structure. 2017.

712   32.   Alexander DH, Novembre J, Lange K. Fast model-based estimation of ancestry in unrelated
713   individuals. Genome Res. 2009;19(9):1655–64.

714   33.   Pritchard JK, Stephens M, Rosenberg NA, Donnelly P. Association Mapping in Structured
715   Populations. Am J Hum Genet. 2000;67(1):170–81.

716   34.   Lawson DJ, Hellenthal G, Myers S, Falush D. Inference of population structure using dense
717   haplotype data. PLoS Genet. 2012;8(1).

718   35.   Kwong A, Kang HM, Program TT-O for PM. A robust unified test for Hardy-Weinberg
719   equilibrium in arbitrarily structured populations. In: ASHG 2018 Annual Meeting. ASHG 2018
720   Annual Meeting; 2018.

721   36.   Claes P, Hill H, Shriver MD. Toward DNA-based facial composites: Preliminary results and
722   validation. Forensic Sci Int Genet. 2014;

723   37.   Lippert C, Sabatini R, Maher MC, Kang EY, Lee S, Arikan O, et al. Identification of individuals by
724   trait prediction using whole-genome sequencing data. Proc Natl Acad Sci. 2017;

725   38.   Claes P, Vandermeulen D, De Greef S, Willems G, Clement JG, Suetens P. Computerized
726   craniofacial reconstruction: Conceptual framework and review. Forensic Science International.
727   2010.

728   39.   Claes P, Vandermeulen D, De Greef S, Willems G, Clement JG, Suetens P. Bayesian estimation
729   of optimal craniofacial reconstructions. Forensic Sci Int. 2010;

730   40.   Claes P, Walters M, Gillett D, Vandermeulen D, Clement JG, Suetens P. The normal-equivalent:
731   A patient-specific assessment of facial harmony. Int J Oral Maxillofac Surg. 2013;

732   41.   Deng HW, Chen WM, Recker RR. Population admixture: Detection by Hardy-Weinberg test and
733   its quantitative effects on linkage-disequilibrium methods for localizing genes underlying
734   complex traits. Genetics. 2001;

735   42.   Bhatia G, Patterson N, Pasaniuc B, Zaitlen N, Genovese G, Pollack S, et al. Genome-wide
736   comparison of African-ancestry populations from CARe and other cohorts reveals signals of
737   natural selection. Am J Hum Genet. 2011;89(3):368–81.

738   43.   Claes P, Walters M, Clement J. Improved facial outcome assessment using a 3D anthropometric
739   mask. Int J Oral Maxillofac Surg. 2012;

740   44.   Snyders J, Claes P, Vandermeulen D, Suetens P. Non-rigid surface registration algorithms:
741   Technical details and comparison. 2014.

742   45.   Rohlf FJ, Slice D. Extensions of the Procrustes Method for the Optimal Superimposition of
743   Landmarks. Syst Zool. 1990;

744 46. Claes P, Roosenboom J, White JD, Swigut T, Sero D, Li J, et al. Genome-wide mapping of global-
745   to-local genetic effects on human facial shape. Nat Genet. 2018;

746 47. Günther T, Malmström H, Svensson EM, Omrak A, Sánchez-Quinto F, Kılınç GM, et al.
747   Population genomics of Mesolithic Scandinavia: Investigating early postglacial migration routes
748   and high-latitude adaptation. PLOS Biol. 2018 Jan 9;16(1):e2003703.

749
750
751 **Supplementary Materials:**

752
753 ***Supplementary Table S1:*** *Information and references for each of the 8 ancient DNA profiles*.

754
755 ***Supplementary Figure S1:*** *Top eight SUGIBS axes of 1KGP and projections of the PSU cohort*

756
757 ***Supplementary Text S1:*** *Determination of the number of relevant or significant components*

758
759

760 *Figure Captions:*
761

762 **Figure 1:** Robustness against individual outliers during the construction of an ancestry space. Top
763 row, the first two ancestry components for A) PCA, B) MDS, C) UPCA and D) SUGIBS using the
764 CEU and TSI populations from the HapMap 3 project. Bottom row, the first two ancestry
765 components for E) PCA, F) MDS, G) UPCA and H) SUGIBS using the CEU and TSI populations
766 from the HapMap 3 project, but with randomly selected single individuals from four different
767 and additional populations (CHB, GIH, MEX and YRI) as "outliers".
768

769 **Figure 2:** Robustness against batch artefacts during the projection of samples onto an ancestry
770 space. Top row, the first two ancestry components of PCA using the original genotypes A),
771 missing genotypes B) and modified genotypes C). Middle row, the second and third ancestry
772 components of UPCA using the original genotypes D), missing genotypes E) and modified
773 genotypes F). Bottom row, the first two ancestry components of SUGIBS using the original
774 genotypes G), missing genotypes H) and modified genotypes I).
775

776 **Figure 3:** Normalized root-mean-square deviation (NRMSD) of the top eight axes of PCA, UPCA and
777 SUGIBS. NRMSD measures the root-mean-square differences (RMSD), for the modified HGDP
778 population only between the scores on ancestry axes generated using the original genotypes
779 (error free) and the modified genotypes (with simulated errors, A) missing genotypes and B)
780 erroneous genotypes). The RMSD values were normalized by the range of the ancestry axes
781 generated using the original genotypes, so that NRMSD of the three methods (PCA, UPCA and
782 SUGIBS) are comparable.
783

784 **Figure 4:** Capturing simulated admixture in function of F_{st}. X-axis represents the different levels of F_{st}
785 investigated. The Y-axis represents the absolute correlation of the first component in PCA, MDS
786 and Spectral-IBS with the simulated ancestry proportion. The higher the correlation the better
787 a method is able to capture the underlying admixture.
788

789 **Figure 5:** Top eight SUGIBS axes of 1KGP and projections of the PSU cohort. Grouped populations of
790 the 1KGP are coloured dots. The projected PSU cohort are represented by grey dots. The faces
791 illustrate opposing variations along each of the ancestry components and are not associated to
792 any of the 1kG populations in particular (these are shown in Figure 6).
793

794 **Figure 6:** Ancestry population average faces for each of the 26 populations in the 1KGP positioned
795 according to geographical origin. The values for sex, BMI and age in the PLSR model were set to
796 0 (sexless), 20 and 25, respectively.
797

798 **Figure 7:** Ancestral facial reconstructions for eight ancient DNA profiles. For these reconstructions,
799 the sex was known from the DNA profile and taken into account in the PLSR model. The values
800 for BMI and age were 20 and 25, respectively.
801
802